$La_{0.6}Sr_{0.4}Co_{0.2}Fe_{0.8}O_{3-\delta}$ oxygen electrodes for solid oxide cells prepared by polymer precursor and nitrates solution infiltration into gadolinium doped ceria backbone

Aleksander Chrzan [a], Jakub Karczewski [b], Maria Gazda [b], Dagmara Szymczewska [a], Piotr Jasinski [a]

[a] Department of Biomedical Engineering, Faculty of Electronics, Telecommunications and Informatics, Gdańsk University of Technology, Narutowicza 11/12, 80-233 Gdańsk, Poland
[b] Department of Solid State Physics, Faculty of Applied Physics and Mathematics, Gdańsk University of Technology, Narutowicza 11/12, 80-233 Gdańsk, Poland

a b s t r a c t

Infiltration is a method, which can be applied for the electrode preparation. In this paper oxygen electrode is prepared solely by the infiltration of $La_{0.6}Sr_{0.4}Co_{0.2}Fe_{0.8}O_{3-\delta}$ (LSCF) into $Ce_{0.8}Gd_{0.2}O_{2-\delta}$ (CGO) backbone. The use a polymer precursor as an infiltrating medium, instead of an aqueous nitrate salts solution is pre-sented. It is shown that the polymer forms the single-phase perovskite at 600 °C, contrary to the nitrates solution. As a result, obtained area specific resistance (ASR) is lowered from 0.21 Ω cm^2 to 0.16 Ω cm^2 at 600 °C. More than 35% of LSCF in the oxygen electrode decreases the performance.

Keywords: SOFC, SOEC, Infiltrated electrodes, LSCF, Polymer precursor

1. Introduction

Solid oxide fuel cells (SOFCs) are devices of great potential for energy generation from hydrogen [1] and hydrocarbon-based fuels [2]. They also may be utilized in reversed mode, working as solid electrolysis cells (SOEC) [3]. However, for practical applications lowered operating temperatures (preferably no more than 600 °C) and lowered production costs, as well as an increased durability are required [1]. A way to reduce the cost of production is to decrease the amount of catalyst used in electrodes, especially in an oxygen electrode. The oxygen electrode (cathode in SOFC, anode in SOEC) is a significant source of polarization resistance at lowered operating temperatures. Thus, elevated electrochemical activity of the electrode is required. It can be obtained by tailoring the structure and decreasing feature size of the electrode to tens of nanometers. An infiltration is a method of electrode preparation that can satisfy these goals [4]. So far fundamental research concerning the infiltration (impregnation) method for SOFC cath-odes has been conducted by a number of groups [5–13]. It was also shown to work well in the case of SOEC anodes [14–16]. In this method the electrode is fabricated in the following order: i) deposition of the backbone (highly porous, several dozen micrometers thick layer of electrolyte material) on the surface of the electrolyte, ii) high–temperature backbone sintering step, iii) multiple impregnations of the backbone with the infiltrate which contains electrode material (catalyst), iv) low-temperature sintering step in order to crystallize the electrode material. The infiltrate is a liquid with low viscosity, which easily penetrates the backbone pores. It can be a suspension of catalyst nanoparticles, aqueous solution of nitrate salts, molten nitrate salts, polymer precursor and more [4,11,17]. The infiltration procedure results in a number of advantages over standard electrode deposition methods: i) backbone is basically an extended electrolyte layer which provides exceptionally large contact area with the electrode, similarly to the composite electrodes; ii) there is no relevant thermal expansion coefficient mismatch; iii) mechanical stability is provided by the backbone thus electrode material can be sintered at relatively low temperature; iv) low volumes of the catalyst are required to ensure electron percolation; v) due to lowered heat treatment temperature, more active but unstable at high temperatures materials can be used

as catalysts while the risk of parasitic reactions is reduced; vi) electrode grains can be nanometer–sized providing high active surface area and triple phase boundary (TPB) length. The advantage v) enables usage of unusual materials like $LaNi_{1-x}Co_xO_{3-\delta}$ [16]. However, in that study, as well as in similar research by Samson [6] (concerning $La_{0.6}Sr_{0.4}CoO_{3-\delta}$), SOFC oxygen electrode sintering temperature was insufficient to produce single-phase perovskite. In both studies aqueous nitrate salts solution was used in infiltration, which is the simplest and the most popular method [18]. Sol–gel methods provide the way of obtaining pure perovskites without high–temperature sintering step, one of them being Pechini method [19]. Slight modification of Pechini method enables to use citrate gel containing well dispersed metal cations. After heating above 400 °C the polymer gel matrix oxidises. This leads to the formation of highly homogenous, yet amorphous, mixture of metal compounds. Further heating results in crystallization into a single–phase material [20], at 600 °C in the case of LSCF [21]. It was shown that a polymer precursor may be used as an infiltrating medium in YSZ films preparation by Net Shape Technology [22] or to infiltrate a porous electrode [11]. In the latter, synthesised electrode particles were studied only as an additional catalyst (infiltrated into existing, composite SOFC cathode), without reaching the percolation limit for the electrons. Up to now, the direct comparison of oxygen electrodes prepared only by the infiltration with aqueous nitrate salts solution and with polymer precursor was not shown.

In this study, oxygen electrodes were prepared exclusively by the infiltration. The advantages of using polymer precursor instead of aqueous nitrate salts solution in order to obtain single–phase electrode material were investigated. These two methods of electrode preparation were directly compared. Moreover, the beneficial influence of polymer matrix on the microstructure of the electrode is studied, since it was shown to form mesoporous films [21]. In addition, the influence of sintering temperature and amount of catalytic material in backbone is shown. The state–of–the–art electrode material $La_{0.6}Sr_{0.4}Co_{0.2}Fe_{0.8}O_{3-\delta}$ (LSCF) and $Ce_{0.8}Gd_{0.2}O_{2-\delta}$ (CGO) electrolyte/backbone are used for the sake of simplicity and comparability. Their performance and structure are measured with electrochemical impedance spectroscopy (EIS) (on symmetrical electrode/electrolyte/electrode samples), scanning electron microscopy (SEM) and high temperature x–ray diffraction (HT–XRD). EIS is performed in oxygen atmosphere under open circuit conditions, which makes this study relevant both to SOFC and to SOEC.

2. Experimental

Presented study was performed using symmetric electrode/electrolyte/electrode samples. First, dense electrolyte was prepared using commercial CGO powder (GDC-20K, Daiichi Kigenso Kagaku Kogyo). It was uniaxially pressed (200 MPa) and sintered at 1350 °C for 2 h. Obtained pellets were 13 mm in diameter and 0.6 mm thick. The backbone was deposited using water suspension of the same CGO powder with 10 wt.% amount of powder. During the deposition a single droplet of CGO suspension was dispersed on the pellet surface and dried. The process was repeated until desired mass of the backbone was obtained. Then the procedure was performed on the other side of the pellet. Finally, the whole structure was sintered at 1300 °C for 1 h. The average thickness of the backbone was 75 μm with approximately 60% of porosity. Two types of infiltrates were prepared, aqueous nitrate salts solution [16] and polymer precursor based on modified Pechini method [23]. The aqueous solution consisted of lanthanum, nickel, strontium and iron nitrates (Sigma–Aldrich) dissolved in deionised water with addition of Triton X-100 and urea.

The concentration of metal cations was 2 M. The polymer precursor was prepared by dissolution of citric acid and metal nitrate salts (Sigma–Aldrich) in water. Then it was mixed with ethylene glycol (POCH) and heated on a hotplate to evaporate the water. Viscosity and wetting properties were controlled with 2–etoxyethanol (POCH). The final concentration of metal cations was 0.4 M. During the infiltration procedure, the infiltrate liquid was applied on the backbone surface and penetrated into the backbone due to the capillary forces. Excess of liquid was removed and the sample was dried and pre–calcined at 400 °C with a heating rate of 13 °C per minute. Afterwards, the sample was weighted to control the amount of electrode material infiltrated into the backbone. The infiltration was repeated from 2 (aqueous solution – 14% of LSCF) to 47 times (polymer precursor – 35% of LSCF) on each side in order to obtain required (from 14% to 49%) volume of catalyst in the electrode (calculated LSCF volume divided by the sum of LSCF and backbone volume). It is worth mentioning that during the experiment and annealing at 800 °C mass of the samples decreased as a result of phase content change in catalyst material (e.g. decomposition of strontium carbonate). Subsequently, the final LSCF amount was lower by a factor of 0.85 than initial catalyst amount. However, this study focuses on electrode behaviour after annealing at lower temperatures, therefore the initial amount of catalyst is used in all the figures. For electrochemical measurements, Ag paste was deposited on top of the electrodes for current collection. Additional test with bare backbones and Ag current collectors showed that such a structure has polarization resistance 2 orders of magnitude higher than the one measured for the infiltrated oxygen electrodes, thus Ag current collector does not enhance the polarization resistance of the samples measured in this study.

Scanning electron microscopy (SEM) of the samples was performed with FEI Quanta FEG 250. High temperature X–ray diffractograms (HT–XRD) were recorded with Philips X'Pert Pro (Cu Kα) with high-temperature stage in air. Powders obtained from dried infiltrates were used in HT–XRD measurements. In order to estimate the LSCF phase content in powders prepared from aqueous nitrates solution a semi-quantitative analysis, based on the comparison of the intensity of a single reflection per one phase, was carried out. The reflections with the reference intensity ratio equal 1 were used for each indentified phase. It was also assumed that absorption coefficients of the multiphase material and the constituent phases are similar. This assumption may be considered as fulfilled by the lanthanum oxide as well as the perovskite phases, however the absorption coefficient of strontium carbonate is much lower. So that, the phase content obtained in the case of low heating temperatures (500 °C) should be treated with caution. Electrochemical performance of oxygen electrodes was determined using electrochemical impedance spectroscopy (EIS) with Novocontrol Alpha A impedance analyzer. Spectra were taken using 4-wire configuration, from 1 MHz to 0.1 Hz, with amplitude of 10 mV under open circuit conditions. Inductance of the cell was subtracted from the results. Selected spectra were compared using ADIS (Analysis of Differences in Impedance Spectra) method. It enables graphical comparison between impedance spectra of electrodes with a number of contributions to overall polarization resistance. However, unlike complex-non-linear least squares fitting it is model independent. ADIS method is described in more details in [24].

3. Results and discussion

The results of HT–XRD analysis of material formed from aqueous nitrate salts solution taken at 400 °C, 600 °C and 800 °C is shown in Fig. 1. At 400 °C, just after pre–calcination, prior to the sintering step, nitrate salts form a set of separate metal oxides including: $SrCO_3$, $SrFeO_3$, La_2O_3, Fe_3O_4, Fe_2O_3 and Co_3O_4. No trace of per-
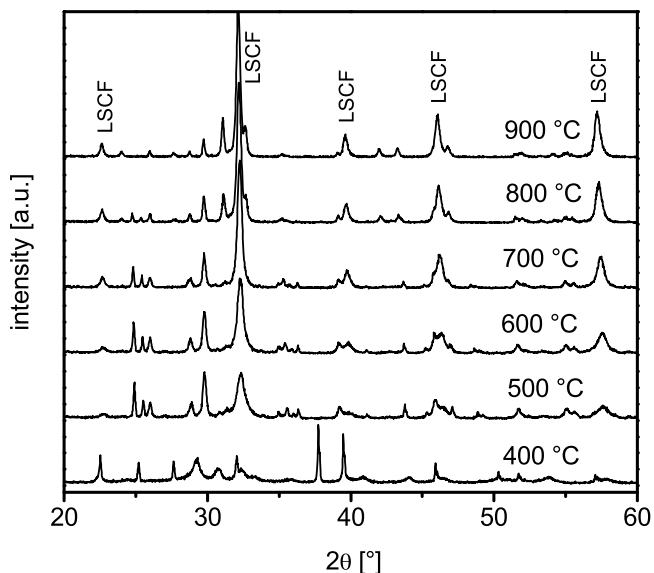
Fig. 1. HT–XRD patterns of material formed from aqueous nitrate salts solution measured at 400, 500, 600, 700, 800 and 900 °C.

Table 1

Approximate phase content for powder obtained from aqueous nitrates solution at different temperatures.

Temperature	500 °C	600 °C	700 °C	800 °C	900 °C
$SrCO_3$	10%	5%	5%	Below 5%	–
La_2O_3	30%	25%	15%	10%	5%
$La_{0.6}Sr_{0.4}Co_{0.2}Fe_{0.8}O_{3-\delta}$	60%	70%	75%	80%	80%
$La_{1.2}Sr_{0.8}Co_{0.5}Fe_{0.5}O_{4-\delta}$	–	–	5%	10%	15%

ovskite LSCF phase is detected. At 500 °C peaks originating from LSCF phase become visible. Additionally there is still a significant amount of La_2O_3 and $SrCO_3$. When heated to higher temperatures secondary phases start to disappear, however peaks corresponding to Ruddlesden–Popper A_2BO_4 phase become visible. The new phase can be identified as $La_{1.2}Sr_{0.8}Co_{0.5}Fe_{0.5}O_{4-\delta}$. Even the pattern taken at 900 °C still shows detectable amount of La_2O_3 and $La_{1.2}Sr_{0.8}Co_{0.5}Fe_{0.5}O_{4-\delta}$. Table 1 sums up estimated phase content of the powder at temperatures above 500 °C. Fig. 2 shows HT–XRD patterns of material formed from polymer precursor. It can be seen that at 400 °C it is amorphous, since only reflections of platinum sample holder are visible. Between 550 °C and 600 °C material crystallizes into the perovskite phase, which is seen in the pattern
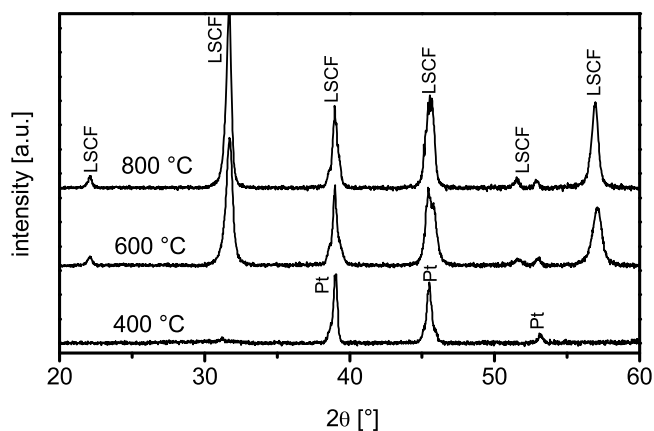

Fig. 2. HT–XRD patterns of material formed from polymer precursor measured at 400, 600 and 800 °C.
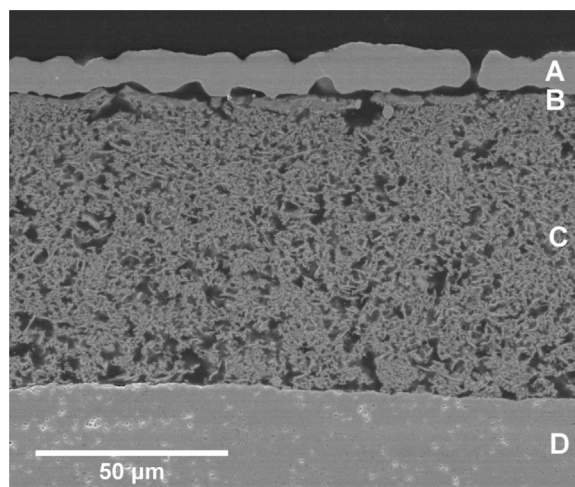

Fig. 3. SEM scan of the polished cross section of symmetrical cell infiltrated and sintered at 800 °C.

taken at 600 °C. After heating to 800 °C the peaks are narrower than these observed at lower temperatures due to the grain growth, and shifted towards lower angles due to the thermal expansion of the crystal lattice. Reflections originating from any secondary phases are not visible.

Fig. 3 shows SEM scan of the studied symmetrical cell infiltrated with aqueous nitrates solution (35% vol.) and sintered at 800 °C. Pores were filled with epoxy to better emphasize the structure. The structure consists of four layers. They are: (A) silver current collector, (B) layer of LSCF over the backbone, (C) backbone infiltrated with LSCF, (D) CGO electrolyte. Porous, flake–like structure of the backbone suspension can be seen. SEM scan of the CGO backbone prior to the infiltration process is and without the epoxy filling shown Fig. 4. Grains have diameter of approximately 0.34 μm (standard deviation of 90 nm), while the backbone surface is well–developed. Sintering temperature of 1300 °C was the lowest, for which backbone showed adequate mechanical stability and sufficient adhesion to the electrolyte. The relatively thin LSCF layer over the backbone, formed during the infiltration process is shown in detail in Fig. 5. The silver current collector was delaminated and no epoxy filling was used. LSCF layer is approximately 1 μm thick and consists of approximately 80 nm grains (standard deviation of 20 nm). It may be beneficial since it serves as a current collector;
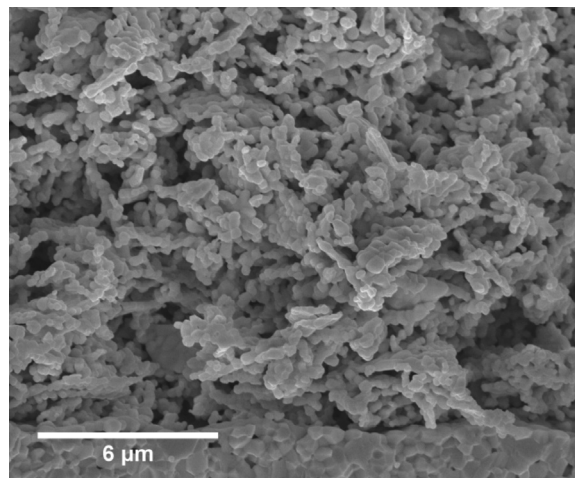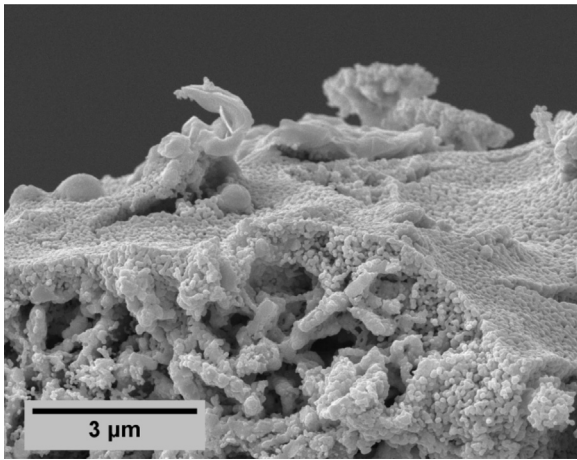

Fig. 4. CGO backbone before the infiltration process.

Fig. 5. LSCF layer formed over the backbone during the infiltration process, sintered at 800 °C.

Fig. 7. Area specific resistance (at 600 °C) of oxygen electrodes prepared with aqueous nitrate salts solution as a function of amount of LSCF in the backbone for samples sintered at 600, 700 and 800 °C.

however, its impact on electrode performance was not investigated in this study.

Fig. 6A shows SEM scan of the backbone infiltrated (35% vol.) with polymer precursor and sintered at 600 °C (the fractured cross section without an epoxy filling). At this point, the morphology seen in SEM scans of aqueous solution and polymer infiltrated backbones is undistinguishable. The infiltrated material covers the backbone with a uniform layer, which appears to be dense. Areas where the material was broken show grainy structure with possible mesopores. Small voids may be created due to solvent and polymer matrix removal. This phenomenon may lead to mesopores formation [21,25]. However, there is no definitive proof in the SEM
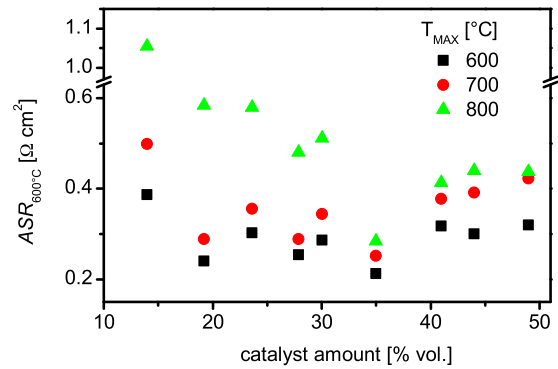
micrographs. In Fig. 6B the sample sintered at 800 °C is shown. The structure of LSCF became porous. This is due to spheroidization of LSCF grains at elevated temperatures [21,26]. It is noteworthy that unlike the aqueous nitrate salts solution, the polymer precursor forms initially amorphous material. Higher strains and organic solvent residues may affect the grain growth, leading to a slightly finer structure [25,27]. The grain size calculated from the image is approximately 61 nm with standard deviation of 13 nm. Fig. 5C shows the backbone infiltrated (35% vol.) with the aqueous nitrate salts solution and sintered at 800 °C. Its structure is very similar to one in Fig. 4B. Slightly smaller porosity of LSCF can be noticed. The grain size calculated from the image is approximately 81 nm with standard deviation of 16 nm.
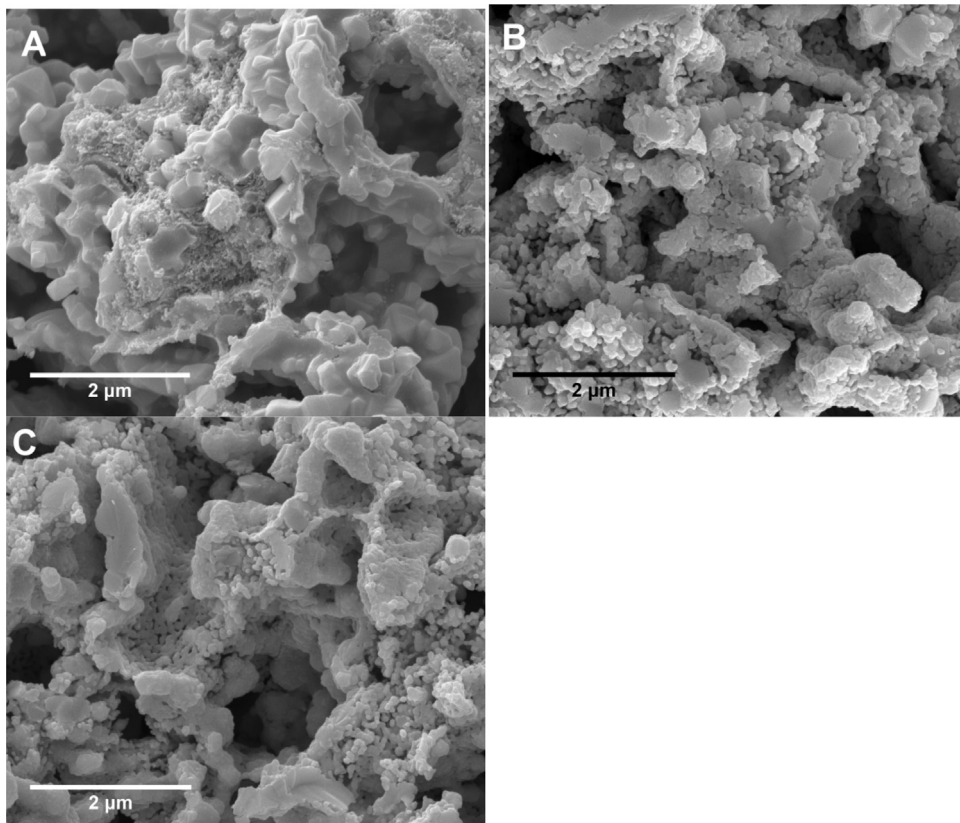

Fig. 6. SEM scan of the fractured cross section of the backbone infiltrated with polymer precursor, sintered at A) 600 °C and B) 800 °C, C) infiltrated with aqueous nitrate salts solution, sintered at 800 °C.
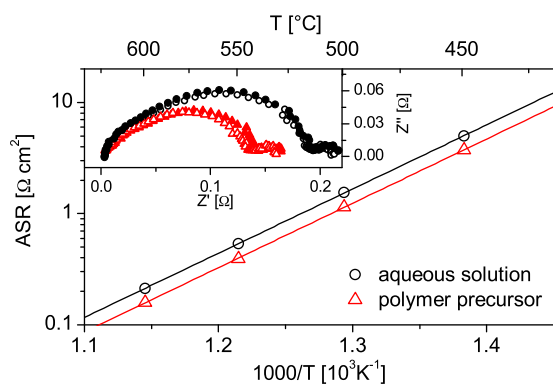
Fig. 8. Arrhenius plots of temperature dependence of ASR for oxygen electrodes prepared using polymer precursor and aqueous nitrate salts solution sintered at 600 °C. Inset: Nyquist plots of EIS measurements at 600 °C. Filled symbols show measurements of the second set of samples.

Fig. 9. ADIS analysis of oxygen electrodes prepared using polymer precursor and aqueous nitrate salts solution sintered and measured at 600 °C.

Fig. 7 shows the plot of area specific resistance (ASR) of oxygen electrodes prepared with aqueous nitrate salts solution as a function of catalyst (LSCF) amount. It is important to note, that "catalyst amount" represents the volume amount of the material created during the infiltration procedure of the electrode. The actual LSCF perovskite phase content, which changes with the annealing temperature, is not taken into account. The ASR values were measured at 600 °C, while the samples were annealed at different maximal temperatures, i.e. 600, 700 and 800 °C. For the lowest amount of LSCF, which is 14%, ASR is the highest, namely $0.39\,\Omega\,cm^2$ after annealing at 600 °C. Additionally, this is the only sample that exceeds $1\,\Omega\,cm^2$ after annealing at 800 °C. This caused by the agglomeration of LSCF grains, which can lead to their separation and drastic drop in number of electron percolation paths [28]. Increase of LSCF amount results in ASR dropping below $0.3\,\Omega\,cm^2$ for samples annealed at 600 °C. The lowest value is obtained with 35% of LSCF, namely $0.21\,\Omega\,cm^2$. At this point, difference between electrochemical behaviour of samples annealed at 700 °C and 800 °C becomes smaller, then between 600 °C and 700 °C. It can be seen that increasing the LSCF amount over 35% vol. slightly increases the polarization resistance. Possibly, the increased amount of LSCF material in the backbone leads to decreased gas permeation and/or decreased triple-phase-boundary due to a better CGO grains coverage. Moreover, the lowest sintering temperature of 600 °C provides the best performance of the oxygen electrode. Therefore, the results obtained for the electrodes with 35% of LSCF sintered at 600 °C are further investigated.

Fig. 8 shows Arrhenius plots of temperature dependence of ASR for oxygen electrodes prepared using polymer precursor and aqueous nitrate salts solution sintered at 600 °C. While they have the same overall activation energy (1.15 ± 0.01 eV), ASR of the electrode prepared through the infiltration of polymer precursor is the lowest, e.g. $0.16\,\Omega\,cm^2$ vs. $0.21\,\Omega\,cm^2$ at 600 °C. These impedance spectra are plotted in the inset, with series resistance subtracted. The inset also contains spectra of the second set of samples, which are hardly different. Polarization resistance was fitted with three CPE-R elements. The high – and middle – frequency elements are associated with the oxygen reduction reaction and transport through the interface, respectively, while the low–frequency element is usually associated with the limited gas diffusion through the electrode [29]. There is no significant difference between the third (diffusive) features of the two spectra. The high and middle frequency features show similar characteristic frequency, which makes them difficult to separate. The difference between these two spectra is shown in ADIS plot in Fig. 9. This plot shows the improvement in the case of the polymer infiltrated electrode in the range of 100 Hz to 10 kHz with maximum at 400 Hz. This range can be
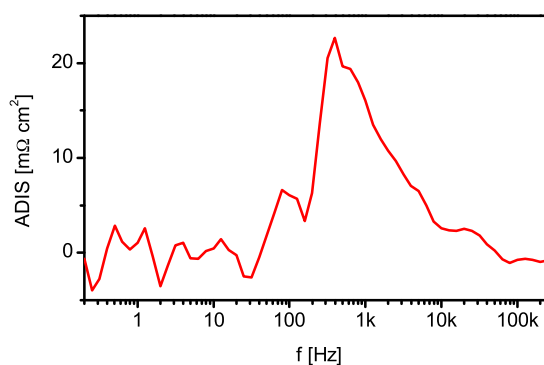
attributed to both oxygen surface exchange and interfacial resistance between LSCF and CGO [29]. However, it is the second feature of the spectrum (often associated with interface resistance [29]) which is the largest one.

ASR at 600 °C presented in this study is slightly lower ($0.16\,\Omega\,cm^2$) than the results showed for optimized, brush painted $La_{0.6}Sr_{0.4}Co_{0.2}Fe_{0.8}O_{3-\delta}$ SOFC cathodes sintered at 800 °C – $0.24\,\Omega\,cm^2$ [21]. Similarly, Hildenbrand showed screen–printed SOFC cathodes with ASR of $0.21\,\Omega\,cm^2$ [30]. Tape–casted, functionally graded SOFC cathodes by Liu had ASR of $\sim 0.5\,\Omega\,cm^2$ at 600 °C [31]. On the other hand, oxygen electrodes with a higher cobalt amount prepared by the infiltration method showed ASR below $0.1\,\Omega\,cm^2$ at 600 °C [32,33]. It should be noted that in the presented study the backbone structure was not optimized which may caused increase in the polarization resistance. Despite this, it was showed that infiltrating of polymer precursor results in better oxygen electrode electrochemical performance compared to these obtained with commonly used aqueous nitrate salts solution.

4. Summary

It was shown that utilization of polymer precursor instead of aqueous nitrate salts solution in infiltration method decreased electrode polarization resistance from $0.21\,\Omega\,cm^2$ to $0.16\,\Omega\,cm^2$ at 600 °C for electrodes with 35% of initial amount of LSCF–based catalyst. Polymer precursor forms the single perovskite phase at temperature as low as 600 °C, contrary to aqueous nitrate salts solution, which is still impure after annealing at 900°. Additionally, it is more likely to obtain mesoporosity due to the polymer matrix decomposition. Amount of 35% of catalyst in the oxygen electrode showed the best performance. However, while the method of infiltration with polymer precursor enables preparation of single-phase, highly performing perovskite oxygen electrodes at temperature as low as 600 °C, it requires significantly more infiltration steps than in the case of aqueous nitrates solution.

Acknowledgements

References

[1] O.Z. Sharaf, M.F. Orhan, An overview of fuel cell technology: fundamentals and applications, Renew. Sustain. Energy Rev. 32 (2014) 810–853, http://dx.doi.org/10.1016/j.rser.2014.01.012.

[2] D. Szymczewska, J. Karczewski, B. Bochentyn, A. Chrzan, M. Gazda, P. Jasinski, Investigation of catalytic layers on anode for solid oxide fuel cells operating with synthetic biogas, Solid State Ionics 271 (2015) 109–115, http://dx.doi.org/10.1016/j.ssi.2014.10.023.

[3] S.D. Ebbesen, X. Sun, M.B. Mogensen, Understanding the processes governing performance and durability of solid oxide electrolysis cells, Faraday Discuss. 182 (2015) 393–422, http://dx.doi.org/10.1039/c5fd00032g.

[4] Y. Huang, J.M. Vohs, R.J. Gorte, SOFC cathodes prepared by infiltration with various LSM precursors, Electrochem. Solid-State Lett. 9 (2006) A237, http://dx.doi.org/10.1149/1.2183867.

[5] M. Shah, S.A. Barnett, Solid oxide fuel cell cathodes by infiltration of La0.6Sr0.4Co0.2Fe0.8O3–δ into Gd-doped Ceria, Solid State Ionics 179 (2008) 2059–2064, http://dx.doi.org/10.1016/j.ssi.2008.07.002.

[6] A.J. Samson, M. Søgaard, R. Knibbe, N. Bonanos, High performance cathodes for solid oxide fuel cells prepared by infiltration of La0.6Sr0.4CoO3-δ into Gd-doped ceria, J. Electrochem. Soc. 158 (2011) B650, http://dx.doi.org/10.1149/1.3571249.

[7] T. Klemensø, C. Chatzichristodoulou, J. Nielsen, F. Bozza, K. Thydén, R. Kiebach, S. Ramousse, Characterization of impregnated GDC nano structures and their functionality in LSM based cathodes, Solid State Ionics 224 (2012) 21–31, http://dx.doi.org/10.1016/j.ssi.2012.07.011.

[8] R. Kiebach, C. Knöfel, F. Bozza, T. Klemensø, C. Chatzichristodoulou, Infiltration of ionic-, electronic- and mixed-conducting nano particles into La0.75Sr0.25MnO3–Y0.16Zr0.84O2 cathodes – a comparative study of performance enhancement and stability at different temperatures, J. Power Sources 228 (2013) 170–177, http://dx.doi.org/10.1016/j.jpowsour.2012.11.070.

[9] R. Küngas, F. Bidrawn, E. Mahmoud, J.M. Vohs, R.J. Gorte, Evidence of surface-reaction rate limitations in SOFC composite cathodes, Solid State Ionics 225 (2012) 146–150, http://dx.doi.org/10.1016/j.ssi.2012.04.030.

[10] M. Shah, P.W. Voorhees, S.A. Barnett, Time-dependent performance changes in LSCF-infiltrated SOFC cathodes: the role of nano-particle coarsening, Solid State Ionics 187 (2011) 64–67, http://dx.doi.org/10.1016/j.ssi.2011.02.003.

[11] S. Lee, K. Gerdes, Functional nanostructure engineering of SOFC cathode by solution infiltration, ECS Electrochem. Lett. 4 (2015) F17–F20, http://dx.doi.org/10.1149/2.0051503eel.

[12] H. Xu, H. Zhang, A. Chu, An investigation of oxygen reduction mechanism in nano-sized LSCF-SDC composite cathodes, Int. J. Hydrogen Energy 41 (2016) 22415–22421, http://dx.doi.org/10.1016/j.ijhydene.2016.09.153.

[13] C. Nicollet, A. Flura, V. Vibhu, A. Rougier, J.-M. Bassat, J.-C. Grenier, An innovative efficient oxygen electrode for SOFC: Pr6O11 infiltrated into Gd-doped ceria backbone, Int. J. Hydrogen Energy 41 (2016) 15538–15544, http://dx.doi.org/10.1016/j.ijhydene.2016.04.024.

[14] K. Chen, N. Ai, S.P. Jiang, Performance and structural stability of Gd0.2Ce0.8O1.9 infiltrated La0.8Sr0.2MnO3 nano-structured oxygen electrodes of solid oxide electrolysis cells, Int. J. Hydrogen Energy 39 (2014) 10349–10358, http://dx.doi.org/10.1016/j.ijhydene.2014.05.013.

[15] Y. Tan, N. Duan, A. Wang, D. Yan, B. Chi, N. Wang, J. Pu, J. Li, Performance enhancement of solution impregnated nanostructured La0.8Sr0.2Co0.8Ni0.2O3-?? oxygen electrode for intermediate temperature solid oxide electrolysis cells, J. Power Sources 305 (2016) 168–174, http://dx.doi.org/10.1016/j.jpowsour.2015.11.094.

[16] A. Chrzan, S. Ovtar, P. Jasinski, M. Chen, A. Hauch, High performance LaNi 1-x Co x O 3-δ (x = 0.4 to 0.7) infiltrated oxygen electrodes for reversible solid oxide cells, J. Power Sources 353 (2017) 67–76, http://dx.doi.org/10.1016/j.jpowsour.2017.03.148.

[17] A. Buyukaksoy, V. Petrovsky, F. Dogan, Efficient cathodes for solid oxide fuel cells prepared by polymeric precursor infiltration, J. Electrochem. Soc. 159 (2012) B68, http://dx.doi.org/10.1149/2.042201jes.

[18] R. Kiebach, P. Zielke, J.V.T. Høgh, K. Thydén, H.J. Wang, R. Barford, P.V. Hendriksen, Infiltration of SOFC stacks: evaluation of the electrochemical performance enhancement and the underlying changes in the microstructure, Fuel Cells 16 (2016) 80–88, http://dx.doi.org/10.1002/fuce.201500107.

[19] M.P. Pechini, N. Adams, Method of preparing lead and alkaline earth titanates and niobates and coating method using the same to form a capacitor, United States Pat. Off. (1967) 01–07. http://scholar.google.com/scholar?hl=en&btnG=Search&q=intitle:Method+of+preparing+lead+and+alkaline+earth+titanates+and+niobates+and+coating+method+using+the+same+to+form+a+capacitor#0.

[20] S. Molin, M. Gazda, P. Jasinski, Conductivity improvement of Ce0.8Gd0.2O1.9 solid electrolyte, J. Rare Earths 27 (2009) 655–660, http://dx.doi.org/10.1016/S1002-0721(08)60309-9.

[21] A. Chrzan, J. Karczewski, D. Szymczewska, P. Jasinski, Nanocrystalline cathode functional layer for SOFC, Electrochim. Acta 225 (2017) 168–174, http://dx.doi.org/10.1016/j.electacta.2016.12.128.

[22] P. Jasinski, V. Petrovsky, T. Suzuki, T. Petrovsky, H.U. Anderson, Electrical properties of YSZ films prepared by net shape technology, J. Electrochem. Soc. 152 (2005) A454, http://dx.doi.org/10.1149/1.1846711.

[23] P. Jasinski, S. Molin, M. Gazda, V. Petrovsky, H.U. Anderson, Applications of spin coating of polymer precursor and slurry suspensions for Solid Oxide Fuel Cell fabrication, J. Power Sources 194 (2009) 10–15, http://dx.doi.org/10.1016/j.jpowsour.2008.12.054.

[24] S.H. Jensen, A. Hauch, P.V. Hendriksen, M. Mogensen, N. Bonanos, T. Jacobsen, A method to separate process contributions in impedance spectra by variation of test conditions, J. Electrochem. Soc. 154 (2007) B1325, http://dx.doi.org/10.1149/1.2790791.

[25] P. Plonczak, M. Joost, J. Hjelm, M. Søgaard, M. Lundberg, P.V. Hendriksen, A high performance ceria based interdiffusion barrier layer prepared by spin-coating, J. Power Sources 196 (2011) 1156–1162, http://dx.doi.org/10.1016/j.jpowsour.2010.08.108.

[26] A. Díaz-Parralejo, A.L. Ortiz, R. Caruso, Effect of sintering temperature on the microstructure and mechanical properties of ZrO2-3mol%Y2O3 sol–gel films, Ceram. Int. 36 (2010) 2281–2286, http://dx.doi.org/10.1016/j.ceramint.2010.07.033.

[27] L.J. Gauckler, D. Beckel, B.E. Buergler, E. Jud, U.P. Muecke, M. Prestat, J.L.M. Rupp, J. Richter, Solid oxide fuel cells systems and materials, Chimia (Aarau) 58 (2004) 837–850, http://dx.doi.org/10.2533/000942904777677047.

[28] J. Ju, Y. Xie, Z. Wang, Y. Zhang, C. Xia, Electrical performance of nano-structured La 0.6 Sr 0.4 Co 0.2 Fe 0.8 O 3-δ impregnated onto yttria-stabilized zirconia backbone, J. Electrochem. Soc. 163 (2016) F393–F400, http://dx.doi.org/10.1149/2.0751605jes.

[29] F. Baumann, J. Fleig, H. Habermeier, J. Maier, Impedance spectroscopic study on well-defined (La,Sr)(Co,Fe)O3–δ model electrodes, Solid State Ionics 177 (2006) 1071–1081, http://dx.doi.org/10.1016/j.ssi.2006.02.045.

[30] N. Hildenbrand, B.A. Boukamp, P. Nammensma, D.H.A. Blank, Improved cathode/electrolyte interface of SOFC, Solid State Ionics 192 (2011) 12–15, http://dx.doi.org/10.1016/j.ssi.2010.01.028.

[31] M. Liu, Z. Liu, M. Liu, L. Nie, Fabrication and characterization of functionally-graded LSCF cathodes by tape casting, Int. J. Hydrogen Energy 38 (2013) 1082–1087, http://dx.doi.org/10.1016/j.ijhydene.2012.10.048.

[32] A.J. Samson, M. Søgaard, P. Hjalmarsson, J. Hjelm, N. Bonanos, S.P.V. Foghmoes, T. Ramos, Durability and performance of high performance infiltration cathodes, Fuel Cells 13 (2013) 511–519, http://dx.doi.org/10.1002/fuce.201200183.

[33] T.E. Burye, J.D. Nicholas, Precursor solution additives improve desiccated La0.6Sr0.4Co0.8Fe0.2O3-x infiltrated solid oxide fuel cell cathode performance, J. Power Sources 301 (2016) 287–298, http://dx.doi.org/10.1016/j.jpowsour.2015.10.012.